

Quantum Enhanced Sensitivity through Many-Body Bloch Oscillations

Hassan Manshouri,^{1,*} Moslem Zarei,^{1,†} Mehdi Abdi,^{2,‡} Sougato Bose,^{3,§} and Abolfazl Bayat^{4,5,¶}

¹*Department of Physics, Isfahan University of Technology, Isfahan 84156-83111, Iran*

²*Wilczek Quantum Center, School of Physics and Astronomy,
Shanghai Jiao Tong University, Shanghai 200240, China*

³*Department of Physics and Astronomy, University College London,
Gower Street, WC1E6BT, London, United Kingdom*

⁴*Institute of Fundamental and Frontier Sciences,
University of Electronic Science and Technology of China, Chengdu 611731, China*

⁵*Key Laboratory of Quantum Physics and Photonic Quantum Information, Ministry of Education,
University of Electronic Science and Technology of China, Chengdu 611731, China*

(Dated: June 21, 2024)

We investigate the sensing capacity of non-equilibrium dynamics in quantum systems exhibiting Bloch oscillations. By focusing on resource efficiency of the probe, quantified by quantum Fisher information, we find different scaling behaviors in two different phases, namely localized and extended. Our results provide a quantitative ansatz for quantum Fisher information in terms of time, probe size, and the number of excitations. In the long-time regime, the quantum Fisher information is a quadratic function of time, touching the Heisenberg limit. The system size scaling drastically depends on the phase changing from super-Heisenberg scaling in the extended phase to size-independent behavior in the localized phase. Furthermore, increasing the number of excitations always enhances the precision of the probe, although, in the interacting systems the enhancement becomes less eminent than the non-interacting probes, which is due to induced localization by interaction between excitations.

Introduction.—The delicate nature of quantum systems makes them naturally suitable for sensing gravitational, magnetic and electric fields with unprecedented precision well beyond the capacity of classical probes [1]. The ultimate precision of a probe for sensing an unknown parameter h , quantified by standard deviation δh , is fundamentally bounded by Cramér-Rao inequality $\delta h \geq 1/\sqrt{\mathcal{M}\mathcal{F}_Q}$, where \mathcal{M} is the number of samples and \mathcal{F}_Q is Quantum Fisher Information (QFI) [2, 3]. The equality can only be achieved when the probe is measured in an optimal basis and thus the QFI indeed dictates the ultimate achievable precision. The performance of a sensor is determined by the scaling of its QFI with respect to resources (e.g. probe size and time), namely $\mathcal{F}_Q \sim L^\beta$, where L is the resource and β is an exponent. While in the absence of quantum features, one can at best achieve $\beta=1$ (i.e. standard limit), in quantum probes, the precision might be enhanced to $\beta > 1$, known as quantum enhanced sensitivity, in which a special case is $\beta=2$ (i.e. Heisenberg limit) [4].

Quantum criticality is known to be instrumental for achieving quantum enhanced sensitivity. In fact, various forms of criticality have been exploited for sensing purposes, including first-order [5–7], second-order [8–24], dissipative [25–34], topological [35–38], Floquet [39, 40], time crystals [41–43], non-Hermitian systems [44–49], and Stark [50–52] phase transitions. However, despite a few attempts for realizing criticality-based sensors [19, 53], their experimental implementation faces real challenges. Normally, in most of such sensors the probe should be initialized in one of its eigenstates, e.g. the ground state, which is very challenging in practice and

may require extra resources to be achieved [18]. In addition, the parameter interval over which such criticality-based probe achieves quantum enhanced sensitivity is often very narrow covering only around the phase transition point. A possible solution for addressing these challenges is to go beyond equilibrium physics and exploit non-equilibrium dynamics of many-body systems [54–58], which is easy to implement in various physical platforms [59–63]. Such systems do not require complex initialization and may allow quantum enhanced sensitivity over a wider range. Several open questions exist, including: (i) what types of non-equilibrium systems may lead to quantum enhanced sensitivity? and (ii) can such probes operate optimally across an entire phase of matter rather than a narrow region around the phase transition point?

Bloch oscillation is a fundamental phenomenon in condensed matter physics in which a particle under the impact of a gradient potential (i.e. a constant force) oscillates in a regular lattice [64]. The gradient potential naturally makes the neighboring lattice sites off-resonant and hence suppresses the tunneling of particles. Unlike classical systems in which particles simply move in the direction of the external force, this suppression of tunneling in quantum systems induces Wannier-Stark localization in the system [65]. The localization properties of Wannier-Stark systems have been extensively studied in both theory [66–89] and experiments [90–93]. Bloch oscillations have also been observed in semiconductor devices [94], optical waveguides [95–97], cold atoms in optical lattices [98] and superconducting simulators [99, 100]. Unlike the conventional second-order

quantum phase transitions which only affect the ground state, the Wannier-Stark localization takes place across the entire spectrum. This implies that the impact of such transition should be observable in non-equilibrium dynamics, where many eigenstates involve. Recently, it has been shown that individual eigenstates of the Wannier-Stark systems can be used for sensing the gradient field with super-Heisenberg precision [50]. A natural question is whether one can exploit experimental-friendly non-equilibrium dynamics of such systems for sensing purposes.

In this letter, we explore the sensing capacity of the Bloch oscillations in single- and many-body Stark systems. We provide a comprehensive analysis for the scaling of the QFI in terms of time, probe size, and the number of excitations. We show that indeed many-body systems with Bloch oscillations may allow for sensing precision with super Heisenberg scaling. Unlike critical probes at equilibrium we do not demand complex initialization and the probe operates optimally over the entire extended phase.

Bloch oscillation in Stark systems.— We establish our theory with the simple case of a single excitation in a one-dimensional lattice of size L described by the Hamiltonian ($\hbar = 1$)

$$H = -J \sum_{l=1}^{L-1} |l\rangle\langle l+1| + |l+1\rangle\langle l| + h \sum_{l=1}^L l|l\rangle\langle l|, \quad (1)$$

where J is the exchange coupling, h is the gradient field and $|l\rangle$ represents the excitation at site l . The gradient field induces a position-dependent energy shift on each site which suppresses the particle tunneling. This leads to the localization of the wave function into a limited number of sites, known as Wannier-Stark localization [65]. In the limit of $L \gg 1$, the eigenstates of Hamiltonian (1), the Wannier-Stark states, are found as $|E_m\rangle = \sum_{l=m}^L \mathcal{J}_l(\frac{2J}{h}) |l\rangle$ whose corresponding eigenvalues are $E_m = mh$ [66]. Here, $\mathcal{J}_l(\cdot)$ are the Bessel function of the first kind. The state $|E_m\rangle$ is a superposition of the states centered at the m th site and spreading to the neighboring sites with the extend about $4J/h$ lattice periods [101]. Any initial state $|\Psi(0)\rangle = \sum_l f_l |l\rangle$, evolves under the action of the Hamiltonian $|\Psi(t)\rangle = e^{-iHt} |\Psi(0)\rangle$ which can be cast into $|\Psi(t)\rangle = \sum_{l,l'=1}^L \mathcal{K}_{l,l'}(t) f_{l'} |l\rangle$ with the evolution propagator $\mathcal{K}_{l,l'}(t) = \sum_{m=1}^L \langle l|E_m\rangle \langle E_m|l'\rangle e^{-iE_m t}$ [66]. Note that in the large L limit, the energies are equidistant, i.e. $\Delta E \equiv E_{m+1} - E_m = h$. Hence, the evolution propagator exhibits a time-periodic behavior with the characteristic time $T_{\text{Bloch}} = 2\pi/h$, that leads to the Bloch oscillations. In order to see the dynamical behavior of the system, we depict $P_l(t) = |\langle l|\Psi(t)\rangle|^2$ as a function of time in Figs. 1(a)-(c) for three different values of h in a system of size $L=100$, initialized at the central site. For larger

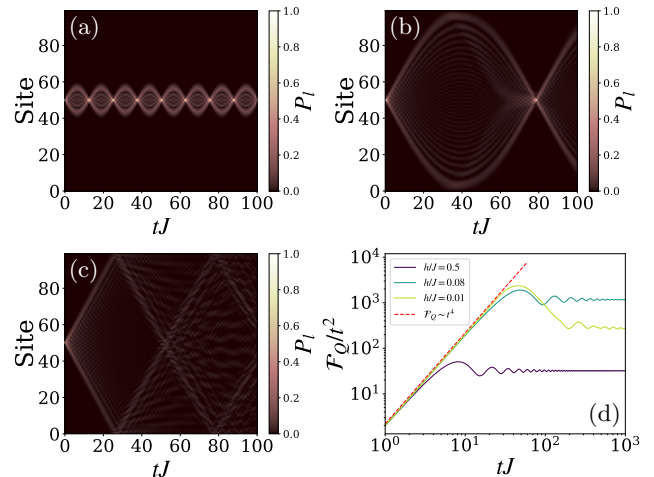


FIG. 1. The time evolution of the population $P_l = |\langle l|\Psi(t)\rangle|^2$ for a system with size $L = 100$, initially localized at $l = 50$, for different phases: (a) $h/J = 0.5$ in the localized phase, (b) $h/J = 0.08$ at the transition point, (c) $h/J = 0.01$ in extended regime. (d) the time evolution of the normalized QFI for different values of h which shows that in the long-time limit, the QFI scales quadratically with time, while at the short-time limit, it scales with time as $\mathcal{F}_Q \sim t^4$.

values of h , shown in Fig. 1(a), one clearly observes periodic spreading of the excitation over a finite distance and returning to its original site. Here, the Bloch oscillations indicate a localized phase. By decreasing h the extent of periodic wave packet spreading increases until $h=h_c \simeq 8J/L$, at which the wave packet delocalizes across the entire system and then localizes back, see Fig. 1(b). This is the point of transition in which the localized phase transforms into an extended phase. Indeed, by further decreasing of h , a new behavior emerges as the excitation spreads across the entire system but does not fully return to its initial localized site, signaling an ergodic behavior [50, 101].

Model 1: Single excitation probe.—A direct consequence of the above evolution is to imprint the information of h in the quantum state $|\Psi(t)\rangle$, which is clearly evidenced in Figs. 1(a)-(c). The sensing capability of such system is quantified by the QFI which can be computed for any pure state $|\Psi\rangle$ as $\mathcal{F}_Q = 4\mathcal{R}e\{\langle \partial_h \Psi | \partial_h \Psi \rangle - \langle \partial_h \Psi | \Psi \rangle \langle \Psi | \partial_h \Psi \rangle\}$ [2]. In Fig. 1(d), we plot the normalized QFI, namely \mathcal{F}_Q/t^2 , as a function of time for three values of h . One notices a rapid growth in time and eventually saturation indicating that after a transient time, the QFI eventually scales quadratically, i.e. $\mathcal{F}_Q \sim t^2$. Crucially, for a given length we observe that the highest long-time value of \mathcal{F}_Q/t^2 is attained when the system is tuned close to its transition point $h=h_c$. Indeed, this is the regime that exhibits the widest sustainable superposition of the wave packet $|\Psi(t)\rangle$. Also, Fig 1(d) shows the size-independent scaling in early times of the QFI as $\mathcal{F}_Q \sim t^4$.

After investigating the time dependence of the QFI,

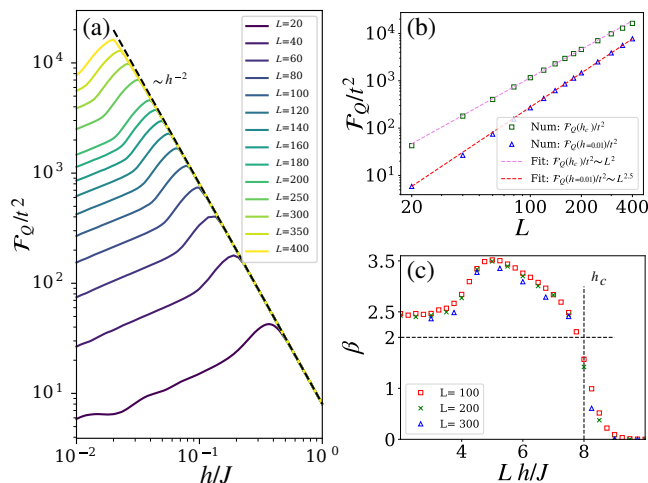


FIG. 2. (a) Long-time behaviour of \mathcal{F}_Q/t^2 as a function of h/J for different system sizes. (b) The scaling of the long-time limit of \mathcal{F}_Q/t^2 with respect to the system size L at the transition point $h=h_c$ (green squares) and deep into the extended phase $h/J=0.01$ (blue triangles). The dashed lines show the best fitting functions. (c) Exponent β as a function of Lh/J for various system sizes L . The transition point is specified at $h_c = 8J/L$ whose corresponding exponent is $\beta=2$.

we now focus on scaling with respect to the probe size L . In Fig. 2(a) we plot the long-time values of \mathcal{F}_Q/t^2 as a function of h for different system sizes. The localization transition points for different system sizes L are clearly identified, which happens around $h_c \simeq 8J/L$. In the localization phase, \mathcal{F}_Q becomes size-independence and scales inversely with square of the gradient field. On the other hand, the QFI becomes size-dependent for $h \leq h_c$. These suggest that

$$\begin{aligned} \mathcal{F}_Q &\sim h^{-2}t^2L^0, & \text{for } h > h_c, \\ \mathcal{F}_Q &\sim t^2L^\beta, & \text{for } h \leq h_c, \end{aligned} \quad (2)$$

where the scaling exponent β may vary with h . Indeed, at the transition point $h_c \simeq 8J/L$, the QFI from both sides of the transition point, given in Eqs. (2), match with each other which results in $\beta=2$. This is confirmed numerically as for different system sizes we find maximized \mathcal{F}_Q/t^2 with respect to h at large time t where \mathcal{F}_Q/t^2 is saturated, see the green squares in Fig. 2(b). Interestingly, in the extended phase, the scaling becomes even better as for $h/J=0.01$ the exponent β increases to $\beta \simeq 2.5$, depicted by blue triangles in Fig. 2(b). Finally, to better understand the metrological aspects of our model we extract the scaling exponent β for arbitrary values of h , see Supplemental Materials (SM) for more details. The results are shown in Fig. 2(c), where one can see a clear super-Heisenberg scaling with $\beta > 2$ in the entire extended phase. The maximum scaling is obtained around $hL/J \simeq 5$ whose exponent is $\beta \simeq 3.5$. As mentioned before, at the transition point $h=h_c$ the QFI scales with Heisen-

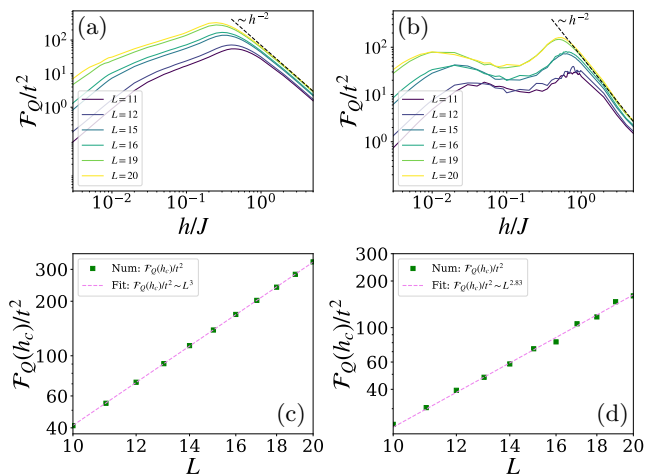


FIG. 3. The normalized QFI for the half-filled initial Neel state as a function of h/J for different system sizes for (a) $\Delta = 0$; and (b) $\Delta = 1$. The long-time limit of \mathcal{F}_Q/t^2 at the transition point $h=h_c$ is plotted as a function of L for: (c) $\Delta = 0$; and (d) $\Delta = 1$.

berg precision, i.e. $\beta=2$, which then drops to $\beta=0$ in the localized phase.

Model 2: many-body probe (half filling).—We now go beyond single excitation and extend our results to systems that consist of multi-particles which may interact with each other. We consider the XXZ Hamiltonian

$$H = -\frac{J}{2} \sum_{l=1}^{L-1} (\sigma_l^x \sigma_{l+1}^x + \sigma_l^y \sigma_{l+1}^y + \Delta \sigma_l^z \sigma_{l+1}^z) + h \sum_{l=1}^L l \sigma_l^+ \sigma_l^-, \quad (3)$$

where Δ represents the strength of the interaction between particles and $\sigma_l^{x,y,z}$ are the Pauli matrices acting on site l . In the single excitation subspace and with $\Delta=0$, the Hamiltonian in Eq. (3) reduces to the single-particle case in Eq. (1). We consider the time evolution of a system initially prepared in a Neel state, i.e. $|\Psi(0)\rangle = |1, 0, \dots, 1, 0\rangle$ for even L and $|\Psi(0)\rangle = |1, 0, \dots, 0, 1\rangle$ for odd L . More details about the time evolution and complex pattern of many-body Bloch oscillations are available in SM. We first put our focus on $\Delta=0$ (non-interacting case) and $\Delta=1$ (isotropic Heisenberg Hamiltonian). The results for the more general case of $0 < \Delta < 1$ are presented and discussed in the next section. In Figs. 3(a) and 3(b), we plot the long time limit of \mathcal{F}_Q/t^2 as a function of h/J for various system sizes L for $\Delta=0$ and $\Delta=1$, respectively. In both interacting and non-interacting regimes, the normalized QFI peaks at the transition point h_c and it shows algebraic decay of the form $\mathcal{F}_Q/t^2 \sim h^{-2}$ in the localized phase, which is similar to the single excitation case. However, unlike the single excitation scenario, even in the localized phase the QFI shows size dependence. Furthermore, one can see that in the presence of interaction, the behavior of

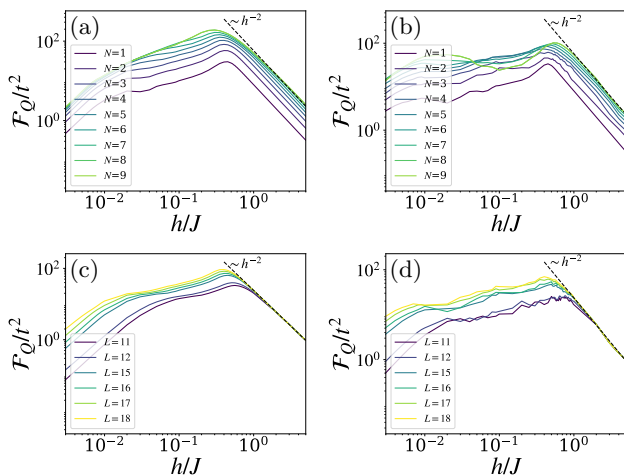


FIG. 4. The long-time limit of \mathcal{F}_Q/t^2 in system of size $L = 17$ for initial states with different excitations as a function of h/J for: (a) $\Delta = 0$; and (b) $\Delta = 1$. The long-time limit of \mathcal{F}_Q/t^2 for a system with the fixed number of excitations $N=3$ and various system sizes for: (c) $\Delta=0$; and (d) $\Delta=1$.

the QFI qualitatively changes as: (i) it shows fluctuations in the vicinity of the transition point; and (ii) its value becomes smaller than the non-interacting case (i.e. $\Delta = 0$). To extract the scaling with system size, in Figs. 3(c) and 3(d) we plot the long-time value of \mathcal{F}_Q/t^2 at $h=h_c$ as a function of system size L for $\Delta=0$ and $\Delta=1$, respectively. Interestingly, in both cases, the scaling suggests $\beta > 2$, which indicates a super-Heisenberg scaling. Especially, in the non-interacting case $\Delta = 0$, it takes the form of $\mathcal{F}_Q(h_c) \sim t^2 L^3$. The difference of $\beta > 2$ here, compared to the single-particle result of $\beta=2$ at the transition point, is related to the number of excitations that will be further explained in the next section.

Effect of excitations.—In the previous section, we focused on the half-filling case, namely $N=L/2$. In this section, we investigate the impact of the number of excitations in more details. For the sake of symmetry, we con-

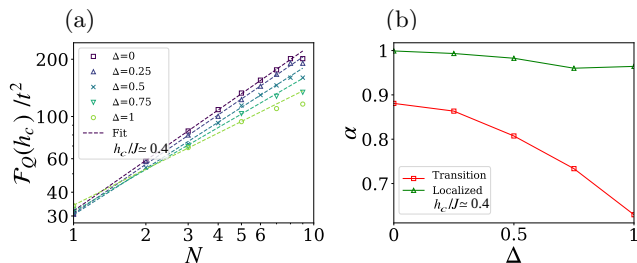


FIG. 5. (a) The scaling of long-time normalized QFI at the transition point with respect to the excitation number N , in a system of size $L = 17$ for different interaction strengths Δ which indicates $\mathcal{F}_Q(h_c)/t^2 \sim N^\alpha$. (b) Exponent α as a function of Δ for two choices of h at the transition points h_c and in the localized phases at $h/J = 5$.

sider odd system sizes L and choose the initial states to be symmetric around the center of the chain. For instance, if the system size is $L=7$ then the initial state with $N = 2$ and $N = 3$ excitations are set to $|0, 0, 1, 0, 1, 0, 0\rangle$ and $|0, 1, 0, 1, 0, 1, 0\rangle$, respectively. In Figs. 4(a) and 4(b) the normalized QFI is plotted for different excitation numbers N in a system of size $L=17$ for $\Delta = 0$ and $\Delta = 1$, respectively. Notably, increasing the excitations always enhances the QFI, indicating better sensitivity. In addition, in the localized phase the QFI shows excitation-dependence. In order to discriminate the QFI enhancement due to the system size from the excitation number, in Figs. 4(c) and 4(d) we plot the long-time behavior of \mathcal{F}_Q/t^2 as a function of h/J for a fixed number of excitation $N=3$ for various choices of L . Interestingly, the size dependence completely disappears for $h > h_c$ indicating that the sensitivity is only enhanced through the number of excitations when the system is in the localized phase (The scaling of the normalized QFI at the transition points in Fig. 4(c) and (d) are discussed in SM). These observations suggest the following ansatzes for the QFI in many-body probes with multiple excitations

$$\begin{aligned} \mathcal{F}_Q &\sim h^{-2} t^2 L^0 N^\alpha, & \text{for } h > h_c, \\ \mathcal{F}_Q &\sim t^2 L^\beta N^\alpha, & \text{for } h \leq h_c, \end{aligned} \quad (4)$$

where α is the exponent which quantifies the dependence on the excitation number. In Fig. 5(a) for a fixed system of size $L=17$, we plot the long-time value of \mathcal{F}_Q/t^2 as a function of N which clearly shows an algebraic growth. To complete the analysis, in Fig. 5(b) the exponent α is depicted as a function of Δ , for two choices of h , one in the localized phase, i.e. $h/J=5$, and one at the transition point $h=h_c$. As the figure shows, while increasing the excitations always enhances the QFI, its rate of enhancement decreases by increasing the interaction strength Δ . This is an interesting observation which can be related to various configurations that the system gets due to the interaction term Δ and effectively enhances the localization [102]. Finally, it is worth emphasizing that in the case of half-filling, namely $N=L/2$, and in the range of $h \leq h_c$ (i.e. extended phase) Eq. (4) suggests that the QFI scales as $\mathcal{F}_Q \sim t^2 L^{\beta+\alpha}$. The main advantage of Eq. (4) is to separate the dependence on L and N . Therefore, one can extract β from the single excitation analysis, shown in Fig. 2(c), and the exponent α can be read from Fig. 5(b). For instance, at the transition point $h=h_c$ the single excitation analysis gives $\beta=2$ and from Fig. 5(b) one reads $\alpha=0.88$ at $\Delta=0$ and $\alpha = 0.63$ at $\Delta=1$. These lead to $\mathcal{F}_Q \sim t^2 L^{2.88}$ and $\mathcal{F}_Q \sim t^2 L^{2.63}$ for $\Delta=0$ and $\Delta=1$, respectively. These scaling functions are very close to the fittings directly extracted in Fig. 3.

Conclusion.—We have studied the metrological aspects of the Bloch oscillations in single- and many-particle Stark systems which support a phase transition, across the entire spectrum, from an extended to a localized phase. Unlike conventional equilibrium criticality-

based quantum sensors, our non-equilibrium probe does not require complex initialization and achieves quantum enhanced sensitivity across the entire extended phase. In addition, our analysis provides an ansatz for the QFI in terms of time, probe size, and number of excitations. In the long-time limit, the QFI scales quadratically with time. In contrast, the precision with respect to the probe size transforms from super-Heisenberg scaling in the extended phase to size-independent behavior in the localized phase. Finally, the number of excitations always enhances the precision of the probe, though, the amount of enhancement depends on the interaction between excitations. Given its time-dependent feature, our work sets the groundstone for further precision measurement experiments, e.g. in gravitometry or electric field sensing.

Acknowledgements.—The authors thank the Center for High Performance Computing at Shanghai Jiao Tong University for providing access to the Siyuan-1 cluster. The work of MA was partially supported by the Yangyang Development Foundation. AB acknowledges support from the National Natural Science Foundation of China (Grants No. 12050410253, No. 92065115, and No. 12274059), and the Ministry of Science and Technology of China (Grant No. QNJ2021167001L). HM acknowledges partial financial support by Iran Optics and Quantum Technologies Development Council.

* h.manshouri@ph.iut.ac.ir

† m.zarei@iut.ac.ir

‡ mehabdi@gmail.com

§ s.bose@ucl.ac.uk

¶ abolfazl.bayat@uestc.edu.cn

- [1] C. L. Degen, F. Reinhard, and P. Cappellaro, Quantum sensing, *Rev. Mod. Phys.* **89**, 035002 (2017).
- [2] M. G. Paris, Quantum estimation for quantum technology, *Int. J. Quantum Inf.* **7**, 125 (2009).
- [3] J. J. Meyer, Fisher Information in Noisy Intermediate-Scale Quantum Applications, *Quantum* **5**, 539 (2021).
- [4] V. Giovannetti, S. Lloyd, and L. Maccone, Quantum-enhanced measurements: beating the standard quantum limit, *Science* **306**, 1330 (2004).
- [5] M. Raghunandan, J. Wrachtrup, and H. Weimer, High-density quantum sensing with dissipative first order transitions, *Phys. Rev. Lett.* **120**, 150501 (2018).
- [6] T. L. Heugel, M. Biondi, O. Zilberberg, and R. Chitra, Quantum transducer using a parametric driven-dissipative phase transition, *Phys. Rev. Lett.* **123**, 173601 (2019).
- [7] L.-P. Yang and Z. Jacob, Engineering first-order quantum phase transitions for weak signal detection, *J. Appl. Phys.* **126**, 174502 (2019).
- [8] P. Zanardi and N. Paunković, Ground state overlap and quantum phase transitions, *Phys. Rev. E* **74**, 031123 (2006).
- [9] P. Zanardi, H. Quan, X. Wang, and C. Sun, Mixed-state fidelity and quantum criticality at finite temperature, *Phys. Rev. A* **75**, 032109 (2007).
- [10] S.-J. Gu, H.-M. Kwok, W.-Q. Ning, H.-Q. Lin, *et al.*, Fidelity susceptibility, scaling, and universality in quantum critical phenomena, *Phys. Rev. B* **77**, 245109 (2008).
- [11] P. Zanardi, M. G. Paris, and L. C. Venuti, Quantum criticality as a resource for quantum estimation, *Phys. Rev. A* **78**, 042105 (2008).
- [12] C. Invernizzi, M. Korbman, L. C. Venuti, and M. G. Paris, Optimal quantum estimation in spin systems at criticality, *Phys. Rev. A* **78**, 042106 (2008).
- [13] S.-J. Gu, Fidelity approach to quantum phase transitions, *Int. J. Mod. Phys. B* **24**, 4371 (2010).
- [14] S. Gammelmark and K. Mølmer, Phase transitions and heisenberg limited metrology in an ising chain interacting with a single-mode cavity field, *New J. Phys.* **13**, 053035 (2011).
- [15] M. Skotiniotis, P. Sekatski, and W. Dür, Quantum metrology for the ising hamiltonian with transverse magnetic field, *New J. Phys.* **17**, 073032 (2015).
- [16] M. M. Rams, P. Sierant, O. Dutta, P. Horodecki, and J. Zakrzewski, At the limits of criticality-based quantum metrology: Apparent super-heisenberg scaling revisited, *Phys. Rev. X* **8**, 021022 (2018).
- [17] B.-B. Wei, Fidelity susceptibility in one-dimensional disordered lattice models, *Phys. Rev. A* **99**, 042117 (2019).
- [18] Y. Chu, S. Zhang, B. Yu, and J. Cai, Dynamic framework for criticality-enhanced quantum sensing, *Phys. Rev. Lett.* **126**, 010502 (2021).
- [19] R. Liu, Y. Chen, M. Jiang, X. Yang, Z. Wu, Y. Li, H. Yuan, X. Peng, and J. Du, Experimental critical quantum metrology with the Heisenberg scaling, *npj Quantum Inf.* **7**, 1 (2021).
- [20] V. Montenegro, U. Mishra, and A. Bayat, Global sensing and its impact for quantum many-body probes with criticality, *Phys. Rev. Lett.* **126**, 200501 (2021).
- [21] S. S. Mirkhalaf, D. B. Orenes, M. W. Mitchell, and E. Witkowska, Criticality-enhanced quantum sensing in ferromagnetic bose-einstein condensates: Role of readout measurement and detection noise, *Phys. Rev. A* **103**, 023317 (2021).
- [22] R. Di Candia, F. Minganti, K. V. Petrovnin, G. S. Paraoanu, and S. Felicetti, Critical parametric quantum sensing, *npj Quantum Information* **9** (2023).
- [23] R. Salvia, M. Mehboudi, and M. Perarnau-Llobet, Critical quantum metrology assisted by real-time feedback control, *Phys. Rev. Lett.* **130**, 240803 (2023).
- [24] L. Garbe, O. Abah, S. Felicetti, and R. Puebla, Exponential time-scaling of estimation precision by reaching a quantum critical point, *Phys. Rev. Res.* **4**, 043061 (2022).
- [25] S. Fernández-Lorenzo and D. Porras, Quantum sensing close to a dissipative phase transition: Symmetry breaking and criticality as metrological resources, *Phys. Rev. A* **96**, 013817 (2017).
- [26] K. Baumann, C. Guerlin, F. Brennecke, and T. Esslinger, Dicke quantum phase transition with a superfluid gas in an optical cavity, *Nature* **464**, 1301 (2010).
- [27] M. P. Baden, K. J. Arnold, A. L. Grimsmo, S. Parkins, and M. D. Barrett, Realization of the Dicke model using cavity-assisted raman transitions, *Phys. Rev. Lett.* **113**, 020408 (2014).
- [28] J. Klinder, H. Keßler, M. Wolke, L. Mathey, and A. Hemmerich, Dynamical phase transition in the open

- dicke model, Proc. Natl. Acad. Sci. U.S.A. **112**, 3290 (2015).
- [29] S. Rodriguez, W. Casteels, F. Storme, N. C. Zambon, I. Sagnes, L. Le Gratiet, E. Galopin, A. Lemaître, A. Amo, C. Ciuti, *et al.*, Probing a dissipative phase transition via dynamical optical hysteresis, Phys. Rev. Lett. **118**, 247402 (2017).
- [30] M. Fitzpatrick, N. M. Sundaresan, A. C. Li, J. Koch, and A. A. Houck, Observation of a dissipative phase transition in a one-dimensional circuit QED lattice, Phys. Rev. X **7**, 011016 (2017).
- [31] J. M. Fink, A. Dombi, A. Vukics, A. Wallraff, and P. Domokos, Observation of the photon-blockade breakdown phase transition, Phys. Rev. X **7**, 011012 (2017).
- [32] T. Ilias, D. Yang, S. F. Huelga, and M. B. Plenio, Criticality-enhanced quantum sensing via continuous measurement, PRX Quantum **3**, 010354 (2022).
- [33] T. Ilias, D. Yang, S. F. Huelga, and M. B. Plenio, Criticality-enhanced electromagnetic field sensor with single trapped ions, npj Quantum Inf. **10**, 36 (2024).
- [34] S. Alipour, M. Mehboudi, and A. T. Rezakhani, Quantum metrology in open systems: Dissipative cramer-rao bound, Phys. Rev. Lett. **112**, 120405 (2014).
- [35] J. C. Budich and E. J. Bergholtz, Non-Hermitian topological sensors, Phys. Rev. Lett. **125**, 180403 (2020).
- [36] S. Sarkar, C. Mukhopadhyay, A. Alase, and A. Bayat, Free-fermionic topological quantum sensors, Phys. Rev. Lett. **129**, 090503 (2022).
- [37] F. Koch and J. C. Budich, Quantum non-Hermitian topological sensors, Phys. Rev. Res. **4**, 013113 (2022).
- [38] M. Yu, X. Li, Y. Chu, B. Mera, F. N. Ünal, P. Yang, Y. Liu, N. Goldman, and J. Cai, Experimental demonstration of topological bounds in quantum metrology, Natl. Sci. Rev. (2024).
- [39] U. Mishra and A. Bayat, Driving enhanced quantum sensing in partially accessible many-body systems, Phys. Rev. Lett. **127**, 080504 (2021).
- [40] U. Mishra and A. Bayat, Integrable quantum many-body sensors for ac field sensing, Sci. Rep. **12**, 1 (2022).
- [41] V. Montenegro, M. G. Genoni, A. Bayat, and M. G. Paris, Quantum metrology with boundary time crystals, Commun. Phys. **6**, 304 (2023).
- [42] R. Yousefjani, K. Sacha, and A. Bayat, Discrete time crystal phase as a resource for quantum enhanced sensing, arXiv:2405.00328 (2024).
- [43] F. Iemini, R. Fazio, and A. Sanpera, Floquet time-crystals as sensors of ac fields, arXiv:2306.03927 (2023).
- [44] J. Wiersig, Enhancing the sensitivity of frequency and energy splitting detection by using exceptional points: application to microcavity sensors for single-particle detection, Phys. Rev. Lett. **112**, 203901 (2014).
- [45] Z.-P. Liu, J. Zhang, i. m. c. K. Özdemir, B. Peng, H. Jing, X.-Y. Lü, C.-W. Li, L. Yang, F. Nori, and Y.-x. Liu, Metrology with \mathcal{PT} -symmetric cavities: Enhanced sensitivity near the \mathcal{PT} -phase transition, Phys. Rev. Lett. **117**, 110802 (2016).
- [46] W. Langbein, No exceptional precision of exceptional-point sensors, Phys. Rev. A **98**, 023805 (2018).
- [47] H.-K. Lau and A. A. Clerk, Fundamental limits and non-reciprocal approaches in non-hermitian quantum sensing, Nature Communications **9** (2018).
- [48] M. Zhang, W. Sweeney, C. W. Hsu, L. Yang, A. D. Stone, and L. Jiang, Quantum noise theory of exceptional point amplifying sensors, Phys. Rev. Lett. **123**, 180501 (2019).
- [49] C. Chen, L. Jin, and R.-B. Liu, Sensitivity of parameter estimation near the exceptional point of a non-hermitian system, New Journal of Physics **21**, 083002 (2019).
- [50] X. He, R. Yousefjani, and A. Bayat, Stark localization as a resource for weak-field sensing with super-Heisenberg precision, Phys. Rev. Lett. **131**, 010801 (2023).
- [51] R. Yousefjani, X. He, and A. Bayat, Long-range interacting Stark many-body probes with super-Heisenberg precision, Chin. Phys. B **32**, 100313 (2023).
- [52] R. Yousefjani, X. He, A. Carollo, and A. Bayat, Nonlinearity-enhanced quantum sensing in stark probes, arXiv:2404.10382 (2024).
- [53] D.-S. Ding, Z.-K. Liu, B.-S. Shi, G.-C. Guo, K. Mølmer, and C. S. Adams, Enhanced metrology at the critical point of a many-body rydberg atomic system, Nat. Phys. **18**, 1447 (2022).
- [54] A. V. Balatsky, P. Roushan, J. Schaltegger, and P. J. Wong, Quantum sensing from gravity as universal dephasing channel for qubits, arXiv:2406.03256 (2024).
- [55] A. Bhattacharyya, D. Saha, and U. Sen, Even-body interactions favour asymmetry as a resource in metrological precision, arXiv:2401.06729 (2024).
- [56] A. Bhattacharyya, A. Ghoshal, and U. Sen, Restoring metrological quantum advantage of measurement precision in a noisy scenario, Phys. Rev. A **109**, 052626 (2024).
- [57] V. Montenegro, G. S. Jones, S. Bose, and A. Bayat, Sequential measurements for quantum-enhanced magnetometry in spin chain probes, Phys. Rev. Lett. **129**, 120503 (2022).
- [58] Y. Yang, V. Montenegro, and A. Bayat, Extractable information capacity in sequential measurements metrology, Phys. Rev. Research **5**, 043273 (2023).
- [59] M. Rispoli, A. Lukin, R. Schittko, S. Kim, M. E. Tai, J. Léonard, and M. Greiner, Quantum critical behaviour at the many-body localization transition, Nature **573**, 385 (2019).
- [60] J. Franke, S. R. Muleady, R. Kaubruegger, F. Kranzl, R. Blatt, A. M. Rey, M. K. Joshi, and C. F. Roos, Quantum-enhanced sensing on optical transitions through finite-range interactions, Nature **621**, 740 (2023).
- [61] X. Mi, M. Sonner, M. Y. Niu, K. W. Lee, B. Foxen, R. Acharya, I. Aleiner, T. I. Andersen, F. Arute, K. Arya, *et al.*, Noise-resilient edge modes on a chain of superconducting qubits, Science **378**, 785 (2022).
- [62] M. Gong, S. Wang, C. Zha, M.-C. Chen, H.-L. Huang, Y. Wu, Q. Zhu, Y. Zhao, S. Li, S. Guo, *et al.*, Quantum walks on a programmable two-dimensional 62-qubit superconducting processor, Science **372**, 948 (2021).
- [63] T. Kohlert, S. Scherg, P. Sala, F. Pollmann, B. Hebbe Madhusudhana, I. Bloch, and M. Aidelsburger, Exploring the regime of fragmentation in strongly tilted fermi-hubbard chains, Phys. Rev. Lett. **130**, 010201 (2023).
- [64] F. Bloch, Über die quantenmechanik der elektronen in kristallgittern, Zeitschrift für physik **52**, 555 (1929).
- [65] G. H. Wannier, Wave functions and effective Hamiltonian for Bloch electrons in an electric field, Phys. Rev. **117**, 432 (1960).
- [66] H. Fukuyama, R. A. Bari, and H. C. Fogedby, Tightly

- bound electrons in a uniform electric field, *Phys. Rev. B* **8**, 5579 (1973).
- [67] M. Holthaus, G. Ristow, and D. Hone, Random lattices in combined ac and dc electric fields: Anderson vs. Wannier-Stark localization, *EPL* **32**, 241 (1995).
- [68] A. Kolovsky and H. Korsch, Bloch oscillations of cold atoms in two-dimensional optical lattices, *Phys. Rev. A* **67**, 063601 (2003).
- [69] A. R. Kolovsky, Interplay between Anderson and Stark localization in 2d lattices, *Phys. Rev. Lett.* **101**, 190602 (2008).
- [70] A. R. Kolovsky and E. N. Bulgakov, Wannier-Stark states and Bloch oscillations in the honeycomb lattice, *Phys. Rev. A* **87**, 033602 (2013).
- [71] E. van Nieuwenburg, Y. Baum, and G. Refael, From Bloch oscillations to many-body localization in clean interacting systems, *Proc. Natl. Acad. Sci. U.S.A.* **116**, 9269 (2019).
- [72] M. Schulz, C. Hooley, R. Moessner, and F. Pollmann, Stark many-body localization, *Phys. Rev. Lett.* **122**, 040606 (2019).
- [73] L.-N. Wu and A. Eckardt, Bath-induced decay of Stark many-body localization, *Phys. Rev. Lett.* **123**, 030602 (2019).
- [74] D. S. Bhakuni, R. Nehra, and A. Sharma, Drive-induced many-body localization and coherent destruction of Stark many-body localization, *Phys. Rev. B* **102**, 024201 (2020).
- [75] D. S. Bhakuni and A. Sharma, Stability of electric field driven many-body localization in an interacting long-range hopping model, *Phys. Rev. B* **102**, 085133 (2020).
- [76] R. Yao and J. Zakrzewski, Many-body localization of bosons in an optical lattice: Dynamics in disorder-free potentials, *Phys. Rev. B* **102**, 104203 (2020).
- [77] T. Chanda, R. Yao, and J. Zakrzewski, Coexistence of localized and extended phases: Many-body localization in a harmonic trap, *Phys. Rev. Res.* **2**, 032039 (2020).
- [78] S. R. Taylor, M. Schulz, F. Pollmann, and R. Moessner, Experimental probes of Stark many-body localization, *Phys. Rev. B* **102**, 054206 (2020).
- [79] Y.-Y. Wang, Z.-H. Sun, and H. Fan, Stark many-body localization transitions in superconducting circuits, *Phys. Rev. B* **104**, 205122 (2021).
- [80] L. Zhang, Y. Ke, W. Liu, and C. Lee, Mobility edge of Stark many-body localization, *Phys. Rev. A* **103**, 023323 (2021).
- [81] R. Yao, T. Chanda, and J. Zakrzewski, Many-body localization in tilted and harmonic potentials, *Phys. Rev. B* **104**, 014201 (2021).
- [82] E. V. Doggen, I. V. Gornyi, and D. G. Polyakov, Many-body localization in a tilted potential in two dimensions, *Phys. Rev. B* **105**, 134204 (2022).
- [83] G. Zisling, D. M. Kennes, and Y. B. Lev, Transport in Stark many-body localized systems, *Phys. Rev. B* **105**, L140201 (2022).
- [84] A. L. Burin, Exact solution of the minimalist Stark many-body localization problem in terms of spin-pair hopping, *Phys. Rev. B* **105**, 184206 (2022).
- [85] C. Bertoni, J. Eisert, A. Kshetrimayum, A. Nietner, and S. Thomson, Local integrals of motion and the stability of many-body localization in Wannier-Stark potentials, *Physical Review B* **109**, 024206 (2024).
- [86] I. Lukin, Y. V. Slyusarenko, and A. Sotnikov, Many-body localization in a quantum gas with long-range interactions and linear external potential, *Phys. Rev. B* **105**, 184307 (2022).
- [87] E. Vernek, Robustness of Stark many-body localization in the J_1 - J_2 Heisenberg model, *Phys. Rev. B* **105**, 075124 (2022).
- [88] E. V. H. Doggen, I. V. Gornyi, and D. G. Polyakov, Stark many-body localization: Evidence for Hilbert-space shattering, *Phys. Rev. B* **103**, L100202 (2021).
- [89] A. Sahoo, U. Mishra, and D. Rakshit, Localization-driven quantum sensing, *Phys. Rev. A* **109**, L030601 (2024).
- [90] W. Morong, F. Liu, P. Becker, K. Collins, L. Feng, A. Kyprianidis, G. Pagano, T. You, A. Gorshkov, and C. Monroe, Observation of stark many-body localization without disorder, *Nature* **599**, 393 (2021).
- [91] P. M. Preiss, R. Ma, M. E. Tai, A. Lukin, M. Rispoli, P. Zupancic, Y. Lahini, R. Islam, and M. Greiner, Strongly correlated quantum walks in optical lattices, *Science* **347**, 1229 (2015).
- [92] T. Kohlert, S. Scherg, P. Sala, F. Pollmann, B. H. Madhusudhana, I. Bloch, and M. Aidelsburger, Experimental realization of fragmented models in tilted Fermi-Hubbard chains, *arXiv:2106.15586* (2021).
- [93] A. H. Karamlou, J. Braumüller, Y. Yanay, A. Di Paolo, P. M. Harrington, B. Kannan, D. Kim, M. Kjaergaard, A. Melville, S. Muschinske, *et al.*, Quantum transport and localization in 1d and 2d tight-binding lattices, *npj Quantum Inf.* **8**, 1 (2022).
- [94] K. Leo, P. H. Bolivar, F. Brüggemann, R. Schwedler, and K. Köhler, Observation of bloch oscillations in a semiconductor superlattice, *Solid State Communications* **84**, 943 (1992).
- [95] U. Peschel, T. Pertsch, and F. Lederer, Optical bloch oscillations in waveguide arrays, *Opt. Lett.* **23**, 1701 (1998).
- [96] Z.-K. Jiang, R.-J. Ren, Y.-J. Chang, W.-H. Zhou, Y.-H. Lu, X.-W. Wang, L. Wang, C.-S. Wang, A. S. Soltsev, and X.-M. Jin, Direct observation of dynamically localized quantum optical states, *Phys. Rev. Lett.* **129**, 173602 (2022).
- [97] H. Tang, X.-F. Lin, Z. Feng, J.-Y. Chen, J. Gao, K. Sun, C.-Y. Wang, P.-C. Lai, X.-Y. Xu, Y. Wang, L.-F. Qiao, A.-L. Yang, and X.-M. Jin, Experimental two-dimensional quantum walk on a photonic chip, *Sci. Adv.* **4**, eaat3174 (2018).
- [98] M. Ben Dahan, E. Peik, J. Reichel, Y. Castin, and C. Salomon, Bloch oscillations of atoms in an optical potential, *Phys. Rev. Lett.* **76**, 4508 (1996).
- [99] X.-Y. Guo, Z.-Y. Ge, H. Li, Z. Wang, Y.-R. Zhang, P. Song, Z. Xiang, X. Song, Y. Jin, L. Lu, *et al.*, Observation of bloch oscillations and wannier-stark localization on a superconducting quantum processor, *npj Quantum Information* **7**, 51 (2021).
- [100] Q. Guo, C. Cheng, H. Li, S. Xu, P. Zhang, Z. Wang, C. Song, W. Liu, W. Ren, H. Dong, *et al.*, Stark many-body localization on a superconducting quantum processor, *Phys. Rev. Lett.* **127**, 240502 (2021).
- [101] M. Holthaus and D. W. Hone, Localization effects in ac-driven tight-binding lattices, *Philosophical Magazine B* **74**, 105 (1996).
- [102] R. Yousefjani and A. Bayat, Mobility edge in long-range interacting many-body localized systems, *Phys. Rev. B* **107**, 045108 (2023).

Supplemental Material: Quantum enhance sensitivity through many-body Bloch oscillations

In this supplemental material we provide further information and more details on the variations of the quantum Fisher information (QFI) both in single- and multi-particle cases. We also present additional information on the Bloch oscillations in the many-body case.

SINGLE PARTICLE QFI SCALING

Further details in studying the size-dependence of the QFI that have brought us to Eqs. (2) in the main text are presented in Fig. S1 where we plot the long-time normalized QFI as a function of system size L for different choices of h . Indeed, for any given h , one observes a power law scaling growth of \mathcal{F}_Q/t^2 with respect to L which experiences an enhancement before turning into a plateau around the size $L \simeq 8J/h_c$. Since the transition point depends on the system size the plateau sets on at different L values. One can clearly identify an improved scaling with size close to the transition point.

MANY-BODY BLOCH OSCILLATION

In this section, we present the results of the Bloch oscillations in the many-body case to compare with the single excitation in Fig. 1 in the main text. To see the behavior of the many-body excitation oscillations at different gradient fields, we compute the dynamics of the probability of having an excitation in every site of the system $P_i(t)$. The results are presented in Fig. S2 for the system size $L = 11$ with the initial state $|\Psi_0\rangle = |010101010\rangle$. Figs. S2(a)-(c) are plotted for the non-interacting sites ($\Delta = 0$) in the extended phase, at the transition point and in the localized phase, respectively. In particular, in Figs. S2(a) the extended phase at $h/J = 0.05$ shows only partial excitation revivals for a few sites at the middle of the lattice. However, as in Fig. S2(b) which shows the probabilities at the transition point $h_c/J = 0.4$ (extracted from Fig. 3(a) in the main text) complete revival for all sites are visible at particular times, e.g. at $tJ = 65$. Meanwhile, Fig. S2(c) corresponds to $h/J = 5$ which represents a system in the localized phase.

In Figs. S2(d)-(f) the same analysis performed for the homogeneous Heisenberg model ($\Delta = 1$) are presented for the same initial state. Even though the localized phase exhibits a behavior akin to the non-interacting case, dynamics of the probabilities in the extended phase and at the transition points are dramatically different. As shown in Fig. S2(e) in the transition point where $h_c/J = 0.9$ (see Fig. 3(b) in the main text), a clear separation between ground- and

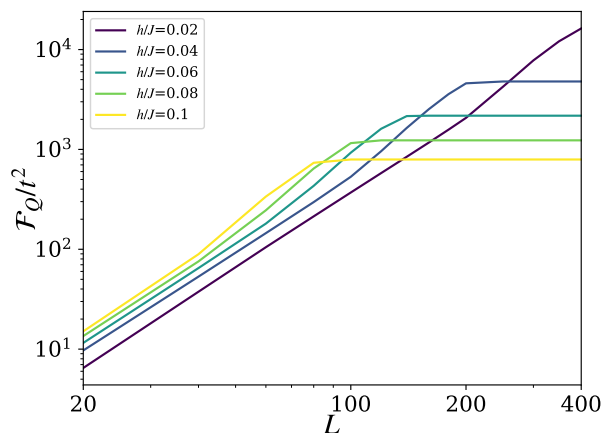


FIG. S1. The normalized QFI for different gradient fields h is plotted as a function of system size L . The plateau for a specific h resembles the localized phase in Fig. 2(a) in the main text.

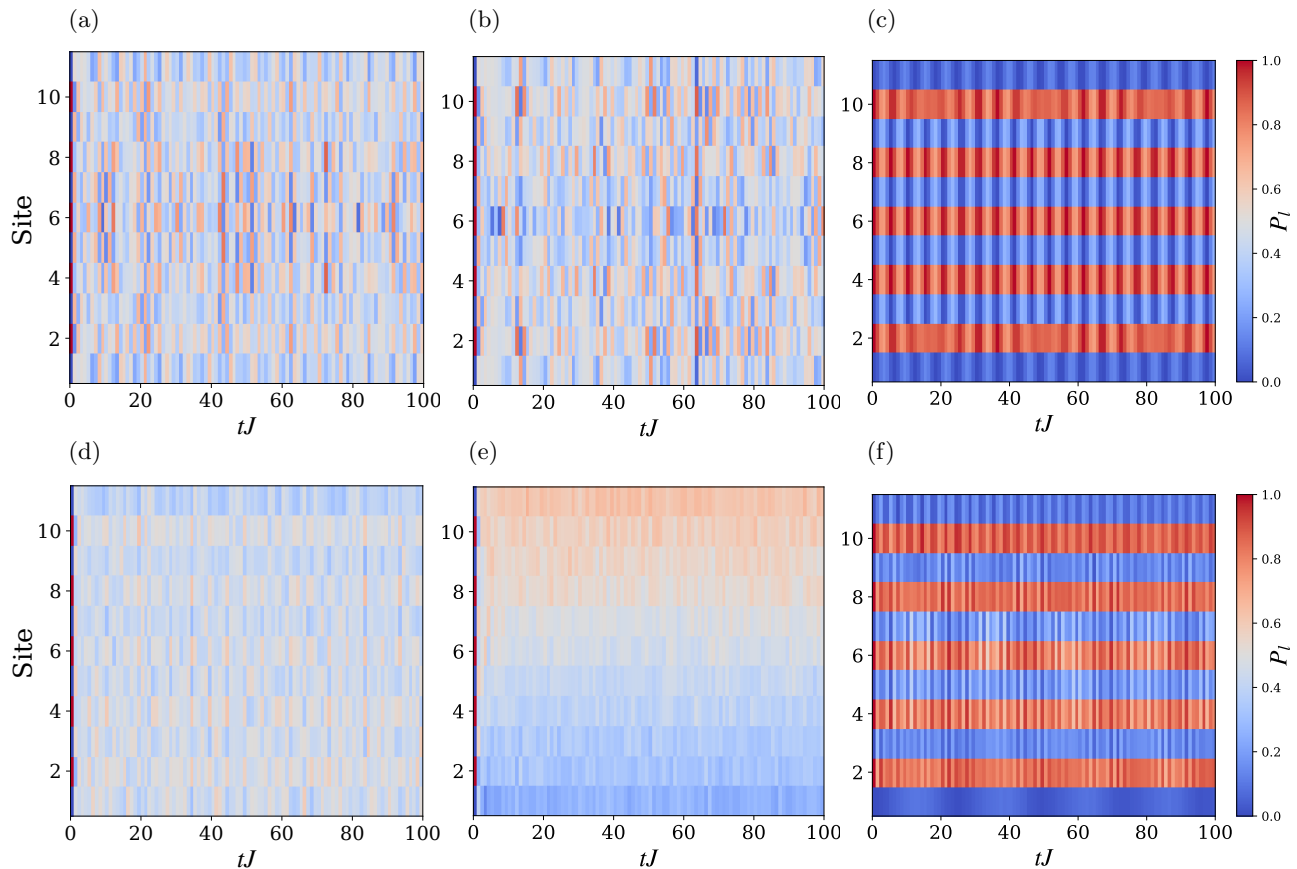


FIG. S2. The probability distribution of each site P_l for the initial state $|\Psi_0\rangle = |010101010\rangle$ are depicted for the system size $L = 11$ for $\Delta = 0$ at (a) $h/J = 0.05$, (b) $h/J = 0.4$ and (c) $h/J = 5$, in extended phase, at the transition point, and in the localized phase, respectively. In (d)-(f) P_l are shown for the Heisenberg Hamiltonian $\Delta = 1$ at $h/J = 0.05$ in the extended phase, $h/J = 0.9$ at the transition point, and $h/J = 5$ in the localized phase, respectively

excited-states is obvious. Comparing Figs. S2(b) and (e) at the transition points, we can deduce that by increasing the interaction strength Δ , the particle excitations tend to occupy sites with higher energies, emerging a clear separation between the excited sites and those who remain in the ground state, see Fig. S2(e).

MANY-BODY QFI SCALING

In studying the single-particle case, we have shown in the main text that the QFI scales as $\mathcal{F}_Q \sim t^2 L^\beta$ where β depends on the phase of the system, which in turn, is determined by h and L [see Fig. 2(c) in the main text]. In particular, we find $\beta=2$ at the transition point. Meanwhile, in the many-body case depending on the number of excitations in the initial state we find the scaling function as $\mathcal{F}_Q \sim t^2 L^\beta N^\alpha$. Unlike β which dramatically changes with the phase, α is almost independent of h . This behavior especially is observed near the transition point. Therefore, for a fixed number of excitations the QFI scales as $\mathcal{F}_Q(h_c) \sim t^2 L^\beta$ with $\beta \approx 2$. To clearly show this point, in Figs. S3(a) and (b) for both $\Delta = 0$ and $\Delta = 1$ we plot the normalized QFI at the transition points $h = h_c$ for a fixed number of excitations ($N=3$) and different system sizes L . The fitting lines confirm the power law scaling $\mathcal{F}_Q(h_c)/t^2 \sim L^\beta$ with $\beta = 2.1$ for $\Delta = 0$ and $\beta = 2.2$ for $\Delta = 1$, which are very close to the value obtained from single-particle case $\beta = 2$.

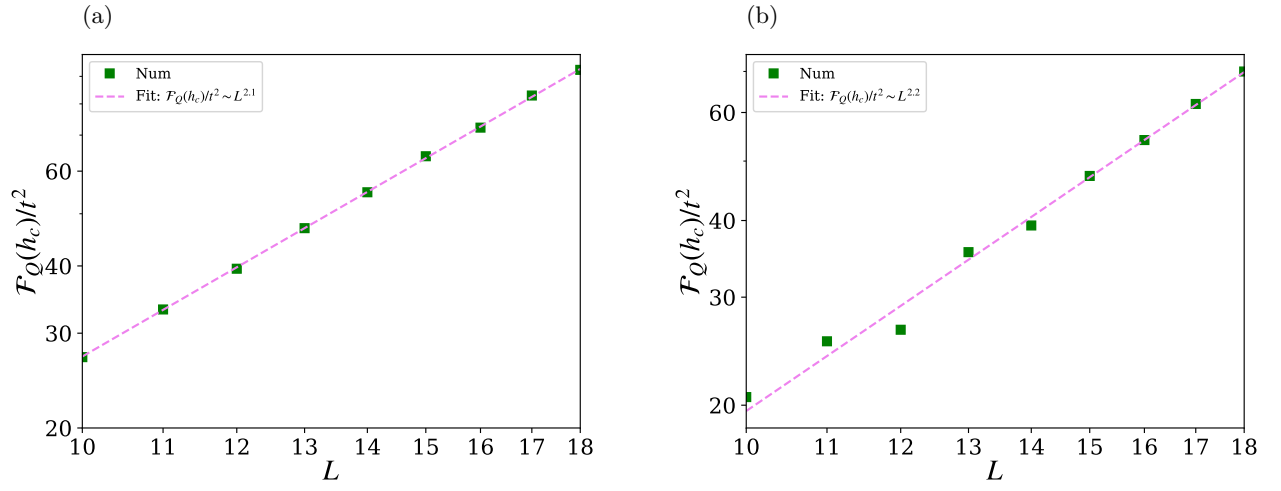


FIG. S3. the normalized QFI at the transition point $\mathcal{F}_Q(h_c)/t^2$ for excitation number $N = 3$ as a function of L for (a) $\Delta = 0$ and (b) $\Delta = 1$. The best fitting exponents for $\mathcal{F}_Q(h_c)/t^2 \sim L^\beta$ are $\beta = 2.1$ for $\Delta = 0$ and $\beta = 2.2$ for $\Delta = 1$.